Iraqi Journal of Physics, 2023 *Vol. 21, No. 4, PP. 1-13*

https://doi.org/10.30723/ijp.v21i4.1150

P-ISSN: 2070-4003
E-ISSN: 2664-5548

Gas Sensor for Hazardous Nitrogen Dioxide Based on TiO_2 Nanotube Synthesis via Electrochemical Method

Mina Mohammed Faris [1a] and Asmaa Kadim Ayal [2b*]
[1]*Department of Chemistry, College of Science, University of Baghdad, Baghdad, Iraq*
[2]*Department of Chemistry, College of Science for Women, University of Baghdad, Baghdad, Iraq*
[a]E-mail: mena.mohammed1105d@sc.uobaghdad.edu.iq
[b*]Corresponding author: asmaakaa_chem@csw.uobaghdad.edu.iq

Abstract

Because of the quick growth of electrical instruments used in noxious gas detection, the importance of gas sensors has increased. X-ray diffraction (XRD) can be used to examine the crystal phase structure of sensing materials, which affects the properties of gas sensing. This contributes to the study of the effect of electrochemical synthesis of titanium dioxide (TiO_2) materials with various crystal phase shapes, such as rutile TiO_2 (R-TiO_2NTs) and anatase TiO_2 (A-TiO_2NTs). In this work, we have studied the effect of voltage on preparing TiO_2 nanotube arrays via the anodization technique for gas sensor applications. The results acquired from XRD, energy dispersion spectroscopy (EDX), and field emission scanning electron microscopy (FE-SEM) elucidate that TiO_2 was created. In addition, systematically examining the gas detection properties was also done. The gas sensor was produced from TiO_2 nanotubes, and the gas-detecting features were directed at nitrogen dioxide (NO_2), which is a hazardous gas. The sensor formed from TiO_2 nanotubes detects NO_2 gas at various temperatures, from room temperature to 300 ^oC, and it has good sensitivity to this gas. The results exhibit that the gas sensor that was synthesized at 30 V has good sensitivity and a short response time at room temperature for NO_2 gas sensing.

Article Info.

Keywords:
TiO_2 Nanotubes, Electrochemical method, Nitrogen Dioxide (NO_2), Gas Sensing, Sensitivity.

Article history:
Received: Jun 18, 2023
Revised: Aug 24, 2023
Accepted: Sep 28, 2023
Published: Dec 01,2023

1. Introduction

The development of portable and low-cost gas sensors with high sensitivity, selectivity, and low working temperatures is highly desirable and still a great challenge. Because of their clear benefits, including their low cost, manufacturing freedom, and excellent thermal and chemical stability, metal oxides appeal as materials for the creation of gas sensing devices [1-3]. For the production of gas monitors, particularly hierarchical nanostructured metal oxides with various shapes are suitable materials.

Utilizing dye-sensitized solar cells, photocatalytic water filtration, capacitive performance, and water splitting to produce hydrogen are just a few examples of how titanium dioxide (TiO_2) is successfully used in environmental and energy production [4-10]. N-type semiconductors are commonly regarded as potential materials for gas detection applications in sensor technology [11-13]. For many distinct gases, including H_2 [14, 15], NO_2 [16, 17], NO_x [18], CO [19], NH_3 [20], H_2S [21-23], and VOCs, they exhibit outstanding sensitivity and selectivity. (i.e., methanol, ethanol, propanol [24, 25], and acetone [26]. It is also commonly noted and researched that useful surface area affects the gas-detecting capabilities of TiO_2 thin films [27].

TiO_2 has a wide band gap and a very high resistivity that can reach 10^8 Ω. However, n-type semiconducting properties can be caused by even a small deviation from stoichiometry due to too many titanium ions [28]. These findings indubitably support the notion that defect disorder and oxygen-to-titanium content ratio stoichiometry play a significant part in the electrical characteristics of TiO_2 [29].

Sol-gel processes [30-32], flame spray synthesis [33], hydrothermal processes [34], electrospinning techniques [35], chemical and physical vapor deposition [36, 37], and thermal, chemical, and electrochemical (anodization) oxidation [38-41] are a few of the different ways TiO_2 can be produced. The phrase "anodization" is a blanket term encompassing a variety of material-treatment procedures, frequently done to produce oxide coatings that enhance the performance of a surface. Nanotubular TiO_2 forms that are completely aligned and self-organized can be produced by anodizing or anodic oxidizing titanium metal sheets.

Although TiO_2 is typically produced as a thin layer, more advanced nanostructures like nanowires, nanorods, nanotubes, and nanoplates have lately been used [35-43]. Microstructural elements such as grain size and surface morphology, which are among the most significant factors affecting a gas sensor's sensitivity, are the source of this research's path.

The large surface area and the shape of tubular structures can increase gas sensitivity. The production of highly ordered nanostructures is another crucial element for the consistency of the functional characteristics of gas sensors. Studies have revealed that titania nanotubes are primarily responsive to hydrogen [42, 43]. The conductance of TiO_2 in air, the sensing signal, the reaction, and the recovery periods are some of the factors that need to be improved in order to broaden the uses of titania nanostructures in the construction of chemical sensors.

Therefore, the present research is focused on the recent synthesis, modifications, and gas sensing properties of titania nanotubes synthesized by an anodization method and fabricated for NO_2 sensing. TiO_2 nanotubes exhibit a good sensing at ambient temperature; therefore, these results contribute to enhanced durability and decreased energy consumption.

2. Experimental Work

2.1. Material

Titanium foils (Flow Serve Company, USA) with a thickness of 0.8 mm and a purity of 99.9% and ethylene glycol (EG) and ammonium fluoride (NH_4F) (AnalaR Chemical Co.) with a purity of 99.5% and 98.0%, respectively, were used. Furthermore, deionized water (DI) (Nanopure Water System, 18 M-cm at 25 °C) was used to yield all of the solutions during the experiment. The voltage source used was a power supply (Laboratory DC Power Supply, TM-605).

2.2. Synthesis Process

In this study, TNT was produced utilizing the electrochemical anodization method. The anodization electrochemical cell's two electrodes are a titanium anode and a graphite cathode (see Fig. 1a). A nanotubular oxide layer is formed on the anode surface when a constant voltage is placed between the anode and cathode due to oxidation, reduction, and field-driven ion diffusion. The anodization parameters influence the characteristics of the produced nanotubes, and the composition of the electrolyte has a significant impact on nanotube production. Fig. 1 depicts the experimental setup utilized for anodization, the titanium plate before anodization, and the titanium plate following anodization. The Ti foil was cleaned by sonication in acetone, isopropanol, and deionized water (DI) for 15 min. Then, 6 M of HNO_3 was used to be chemically etched for 10 min in order to form a smooth surface. After that, the Ti foil was rinsed with DI water and left to dry in the air. The amorphous nanotubes are transformed into crystalline ones by annealing for 2 hrs thermal at 500 ^oC [6].

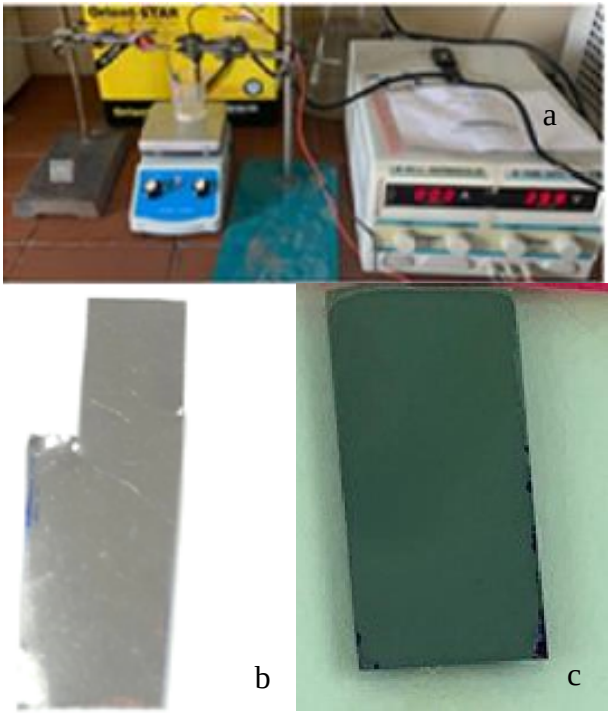

Figure 1: (a) The setup used to create TiO_2 nanotubes, (b) titanium foil before electrochemical anodization, and (c) the formation of TiO_2 nanotubes on the titanium foil after electrochemical anodization.

2.3. Characterization of TiO_2 Nanotube

X-ray diffractometry (XRD) (X'Pert Pro, Philips) was executed in order to determine the structures of the prepared samples. Field emission scanning electron microscopy (FE-SEM) was applied to recognize the morphologies of the TiO_2 nanotube, and the energy dispersive x-ray (EDX) spectrometer was used to analyze the elements. In addition, the Scherrer equation was used to calculate the crystallite sizes of TiO_2 nanotubes:

$$D = \frac{0.89\,\lambda}{\beta\cos\theta} \qquad (1)$$

where cos θ and λ are the incident angles of the X-rays and the wavelength of the X-rays, respectively, while β is the full width at half the maximum of the maximum diffraction peak.

2.4. Gas Sensor System

Fig. 2 represents the sensing test system. It mainly consists of a cylindrical chamber for the test and is made of stainless steel; a gate to allow the gas flow during the test, valve for air flow; electrical connection pins for the heater beneath the chamber base; electrodes with the sensor; a heater with a hot plate; a thermocouple is required for controlling the sensor operation temperature; a digital meter interfaced with a PC for recording the sensor current when the sensor is under dry air fed by a needle valve and flow meter; and current variation when the sensor is subjected to NO_2 gas-air fed by a tube over the sensing film to measure the sensitivity. Response time and recovery time are two significant factors in a gas sensor. The response time is known as the time required by the sensor to acquire 90% of the response on exposure to the target gas. The recovery time is realized as the time required to attain 90% recovery when gas is turned

off [44]. The response and recovery times can be calculated using the following equations:

$$\text{Response time (sec.)} = \left|t_{\text{gas (on)}} - t_{\text{gas (off)}}\right| \times 0.9 \quad (2)$$

$$\text{Recovery time (sec.)} = \left|t_{gas\,(off)} - t_{gas\,(recovery)}\right| \times 0.9 \quad (3)$$

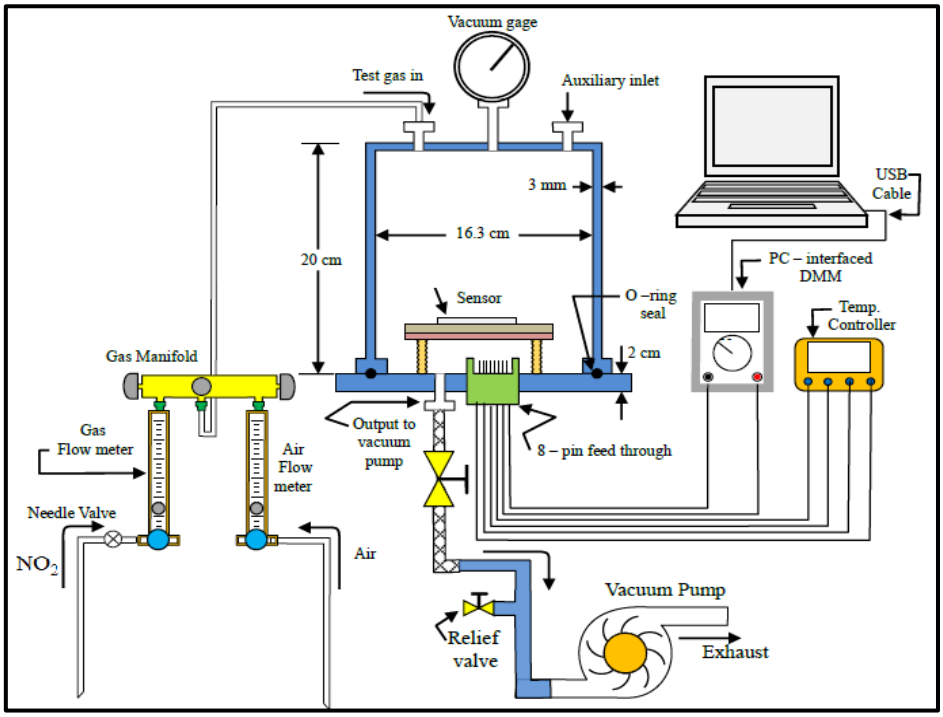

Figure 2: Gas sensor testing system [45].

3. Results and Discussion

3.1. Structural and Morphological Characteristics

Fig. 3 (a, b, c, and d) depicts the FESEM images of titanium oxide nanotube arrays (TiO_2 NTs) produced at various voltages (10, 20, 30, and 40 V) after 2 hrs of annealing. Fig. 3 shows that as the voltage increases, the titanium nanotubes (TNTs) become clearer and the nanotubes become longer. It is possible to detect an improvement in the tubes' diameter and length by changing the anodization voltages [39]. Fig. 4a demonstrates that under this oxidation voltage (10 V), TiO_2 nanotubes have not formed. The form of the tubes becomes more apparent when the voltage is increased. The mechanism of the response shows the start of the growth phase of TiO_2NTs. However, Fig. 3 shows the top view and cross-section of TNT nanotubes produced at different voltages. The lengths and inner and outer diameters of TiO_2 nanotubes may be calculated using the images. Under anodization circumstances, TiO_2 nanotubes had diameters of 26 to 49 nm, respectively, and a length of 2.6 to 3.37 µm. EDX was also used to analyze the components of TiO_2 NTs produced at various anodization voltages after 2hrs of annealing. The TNT elemental weight percentages were stated, as may be seen in Table 1. The elemental mapping and EDX spectra of TiO_2 NTs are also shown in Figs. 4 and 5, which confirm the presence of titanium and oxygen elements. The anodizing electrolyte also contains carbon and nitrogen.

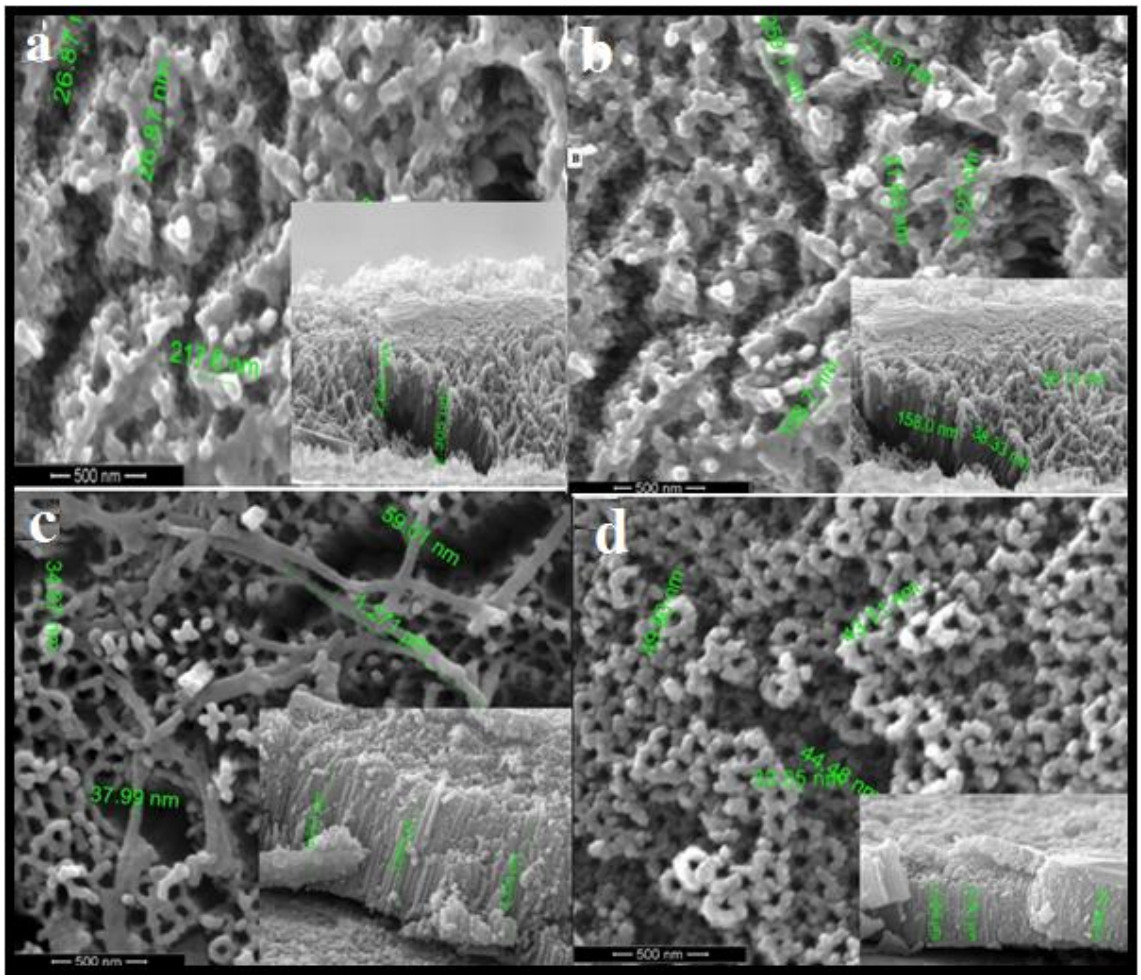

Figure 3: Top view FE-SEM images of TNTs prepared at: (a) 10 V; (b) 20 V; (c) 30 V, and (d) 40 V at 2hr of annealing. Cross-sectionals of the TiO_2 NTs are displayed in inset of the figure.

Table 1: EDS analysis for TiO_2 NTs at different voltages at 2hr of annealing.

Applied voltage (V)	Element	Weight %	Weight % Error
10	C	3.9	0.2
	N	4.8	0.4
	O	30.5	0.9
	Ti	60.9	0.3
20	C	4.7	0.1
	N	4.7	0.2
	O	26.5	1.4
	Ti	64.1	0.2
30	C	4.0	0.1
	N	3.9	0.4
	O	30.9	0.9
	Ti	61.2	0.3
40	C	4.1	0.2
	N	0.6	0.3
	O	29.3	0.9
	Ti	65.9	0.4

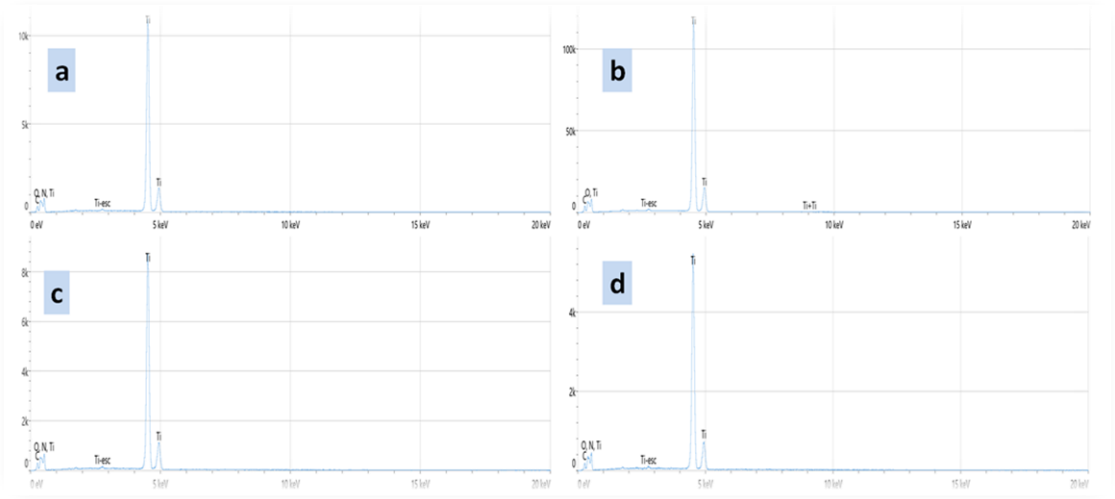

Figure 4: EDX of TiO_2 NTs prepared at: (a) 10 V; (b) 20 V; (c) 30 V, and (d) 40 V at 2h of annealing.

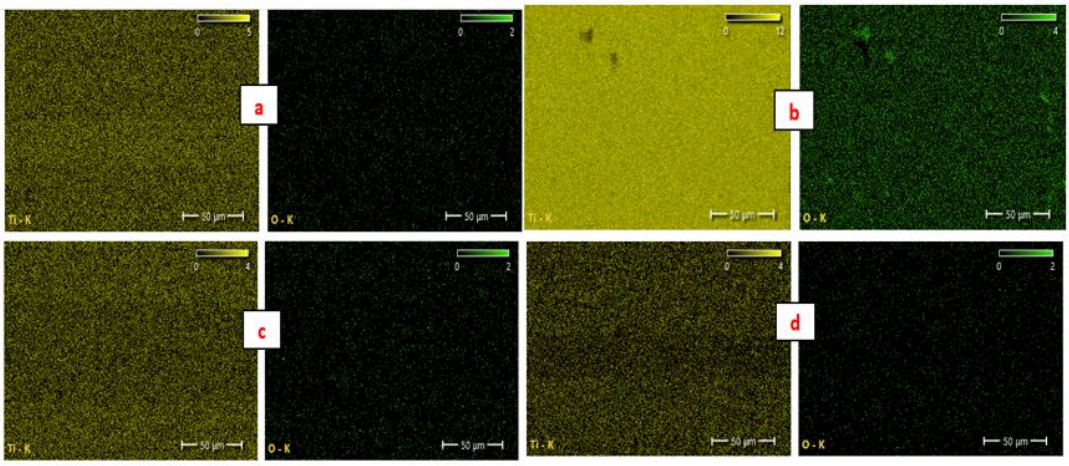

Figure 5: EDX- elemental mapping of TiO_2 NTs prepared at: (a) 10 V; (b) 20 V; (c) 30 V, and (d) 40 V at 2hr of annealing.

Fig. 6 displays the XRD patterns of the synthetic samples at various anodization voltages after 2hrs of annealing. Four diffraction peaks were found for all of the produced samples; these peaks, referred to as anatase, were placed at 24.59°, 37.60°, 47.32°, and 75.55°. According to reference code 00-021-1272, the diffraction peaks were specified in the lattice planes (101), (004), (200), and (215). While Ti has three diffraction peaks, which found in all of the produced samples, these peaks were placed at 39.36°, 53.44° and 70.15°. According to reference code 00-044-1294, the diffraction peaks were specified in the lattice planes (101), (102) and (103). Moreover, no other peaks were detected for rutile TiO_2, implying that the as-prepared sample was of high purity for anatase TiO_2.

Also, the TiO_2 NTs nanotubes are polycrystalline, as shown in Fig. 6. Equation 1 was used to determine the average crystallite size (16.7 nm) from the total width at half the maximum of the TiO_2 anatase (101) diffraction peaks and 2θ.

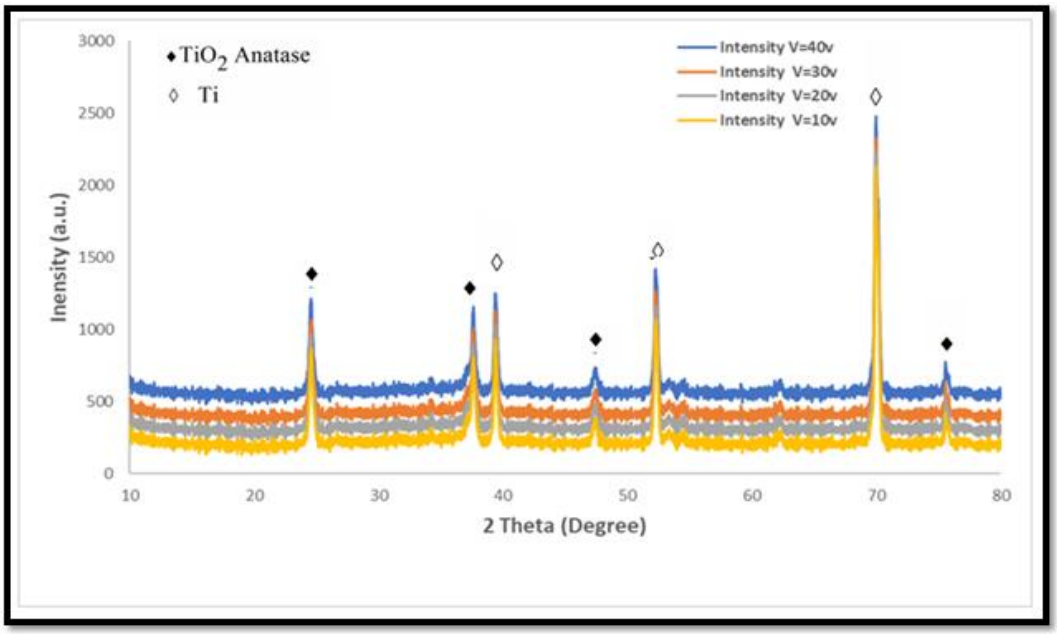

Figure 6: XRD diffractograms of TiO_2 prepared at: (a) 10 V; (b) 20 V; (c) 30 V, and (d) 40 V at 2hrs of annealing.

3.2 Performance of Gas Sensing

Fluctuations in their resistance, which are caused by interactions between semiconductors and ambient gases, provide the foundation for semiconductors' sensing efficiency. The feature of gas sensing is referred to as the dynamic fluctuation of resistance. The sensitivity of the gas sensor for reducing gas is often expressed as the ratio of the resistance in air to the resistance when the gas is present (($R_{on}(\Omega)$-$R_{off}(\Omega)$)/$R_{on}(\Omega)$). In contrast, the definition of an oxidizing gas's response is its resistance in air to resistance in the absence of the gas (($R_{on}(\Omega)$-$R_{off}(\Omega)$)/R_{off} (Ω)) [45]. The results of the interaction of gases and TiO_2 nanotubes revealed that the NO_2 gas decreased the resistance of the TiO_2 nanotube sensor when it was introduced. Air exhibits more resistance than NO_2 gas as a result of an oxide's (n-type) interaction with the oxidation gas, as seen in Figs. 7–10 [46].

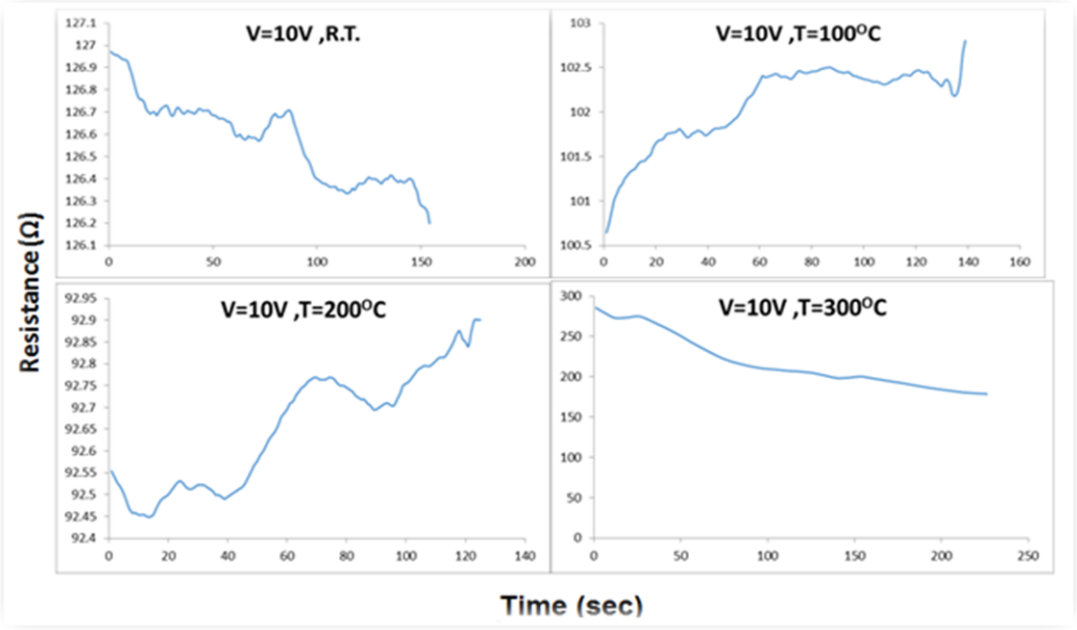

Figure 7: Variation in TiO_2 NTs resistance to NO_2 gas at various operating temperatures.

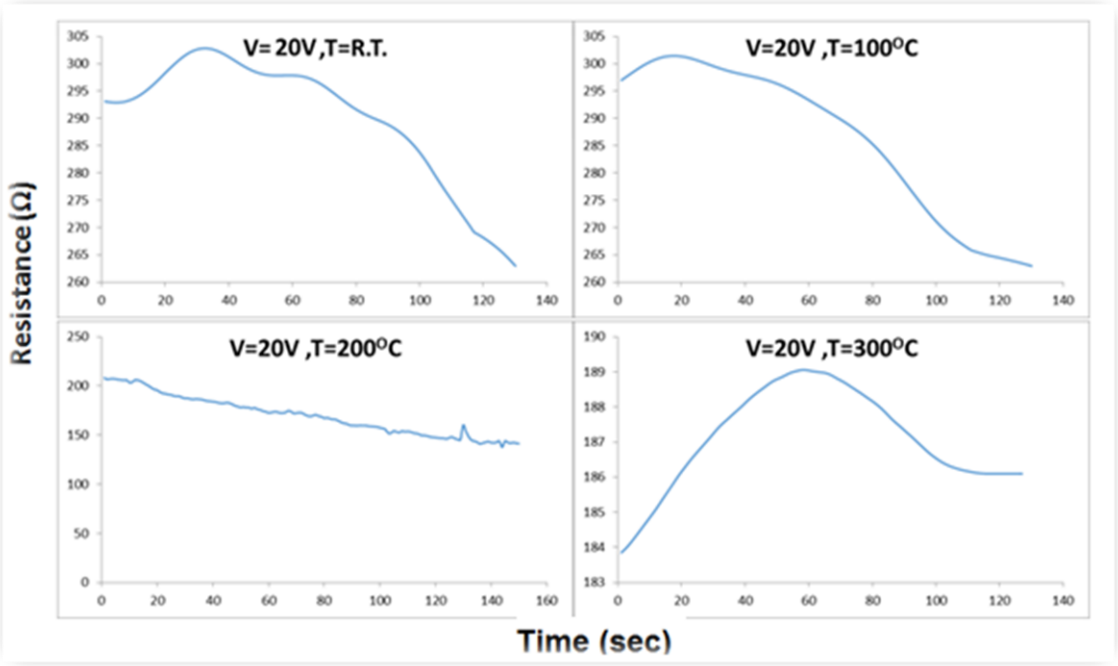

Figure 8: Variation in TiO_2 NTs resistance to NO_2 gas at various operating temperatures.

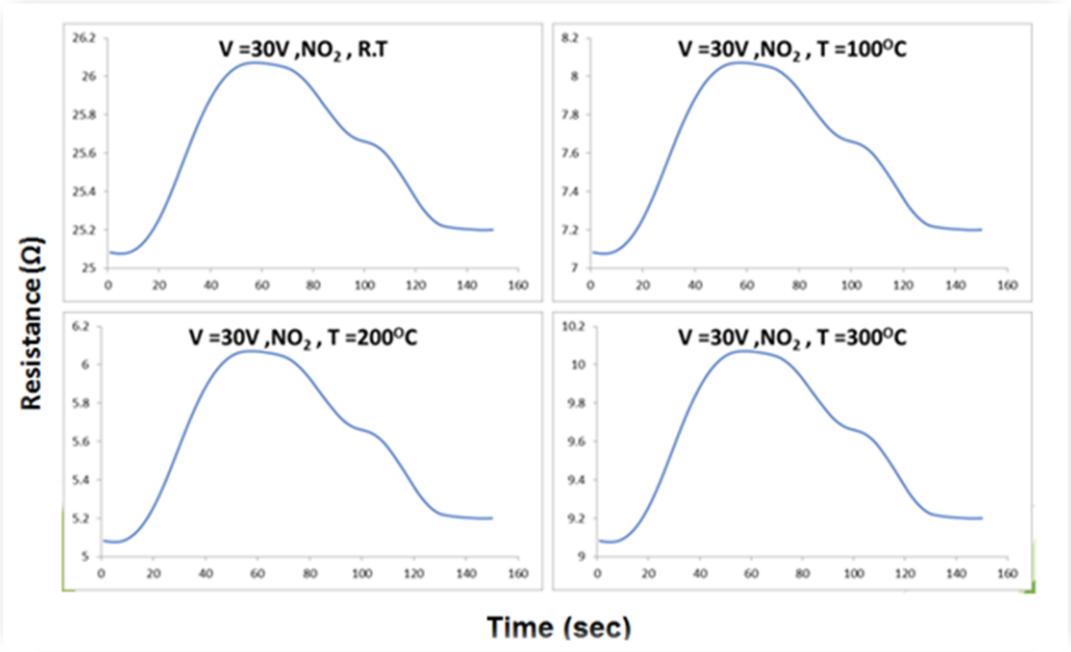

Figure 9: Variation in TiO_2 NTs resistance to NO_2 gas at various operating temperatures.

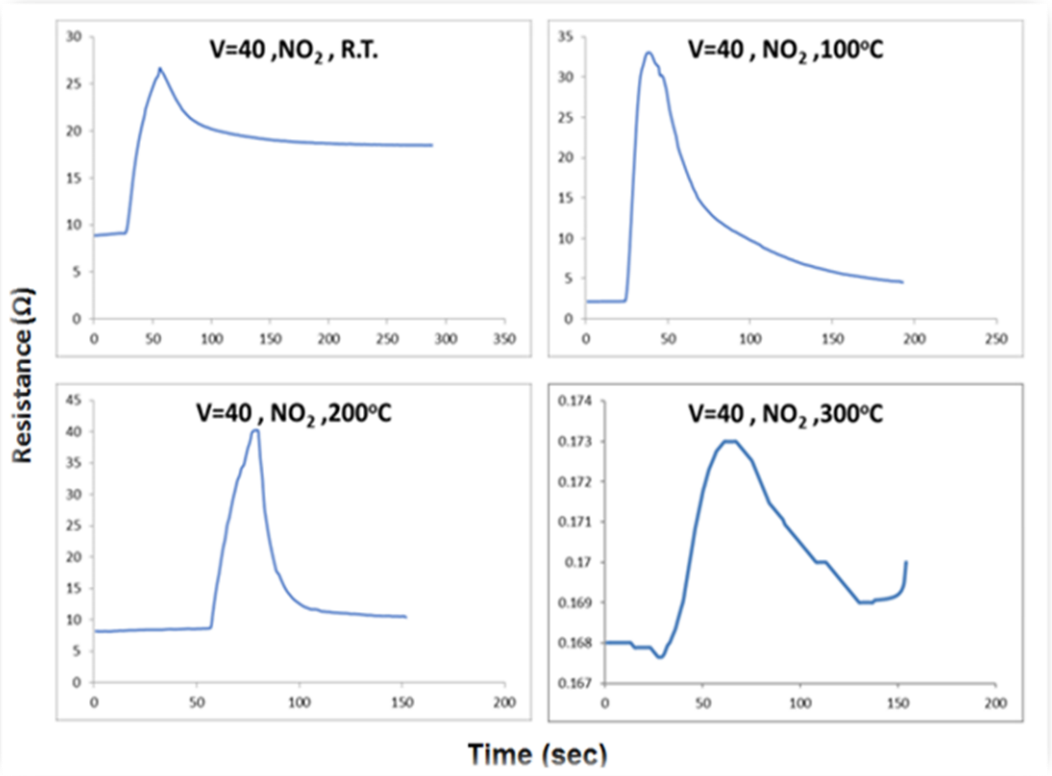

Figure 10: Variation in TiO_2 NTs resistance to NO_2 gas at various operating temperatures.

The primary concerns for gas sensing characteristics, particularly at low working temperatures, are response and recovery times. As illustrated in Fig. 11, the responses of the gas sensors to 45 ppm NO_2 were tested at operating temperatures ranging from ambient temperature to 300°C in order to determine the best temperature for the manufactured TNT gas sensor to function at varied anodizing voltages. In contrast to the TiO_2 NTs sensors created at 10, 20, and 40 V, Fig. 10 shows that the reaction times of NO_2 gases via the TiO_2 NTs prepared at 30 V were faster. Additionally, at the working temperature (room temperature), all the produced samples that were employed as gas sensors exhibited satisfactory reaction times for NO_2 sensing of less than 30 sec. All the gas sensors were manufactured at 10, 20, 30, and 40 V had recovery durations calculated from Eq. (3) that were, respectively, 88.2, 73.8, 92.7, and 66.6 sec at a lower operating temperature. Due to its embedded properties of a large surface area, an improved rate of electron transport, a powerful capacity for adsorption [47], and numerous hollow locations for the gas to diffuse more quickly [48-50], TNTs at 30 volts may be the ideal nanostructure for gas disclosure.

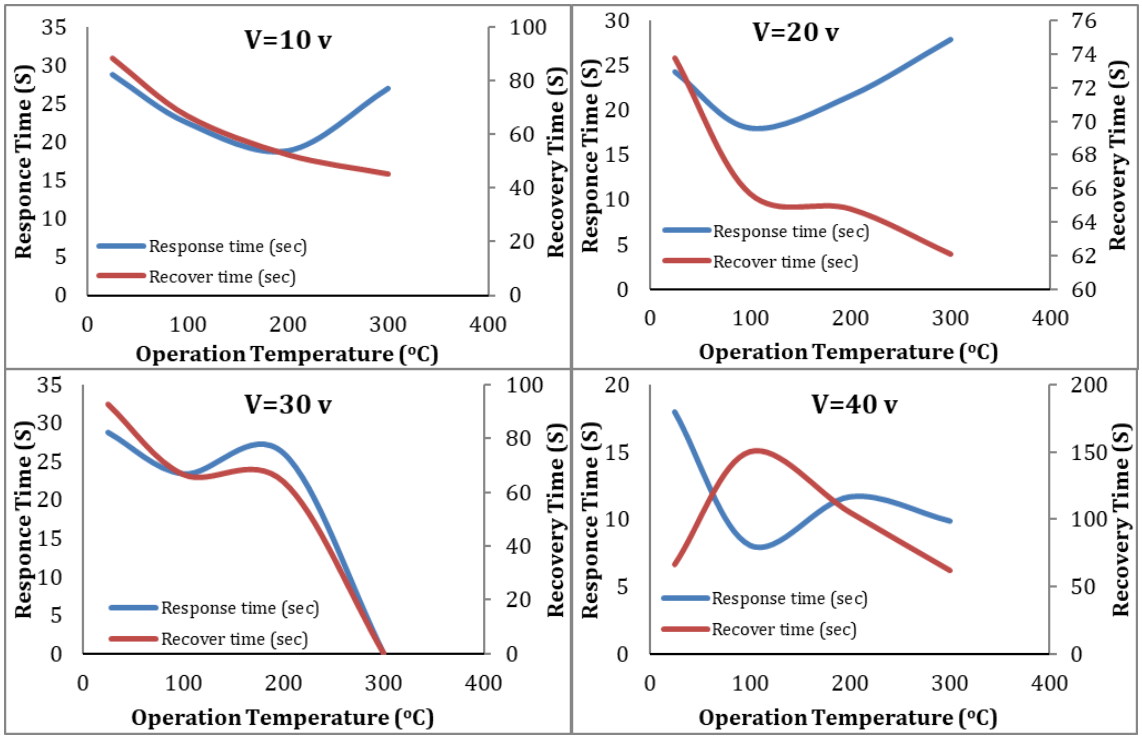

Figure 11: Response and recovery times of TiO_2 NTs prepared at various voltages.

Fig. 12 illustrates the TiO_2 NTs sensor's gas sensitivity to NO_2 at various working temperatures, from room temperature to 300 °C at a 45 ppm NO_2 concentration. The sensitivity of TNTs sensors ranged from roughly 6.060 to 16.903%, with the TiO_2 NTs sensor manufactured at 30 V (for 2 hrs of annealing) have the maximum sensitivity at room temperature at 16.903%. This indicates that the sensitivity of the sensor is significantly impacted by the operating temperature. The TiO_2 NTs sensor had the highest sensitivity at room temperature due to the hollow structures, which helped enhance the gas exposure and made it easy to adsorb and desorb gas molecules [50].

The way TiO_2 NTs gas sensors detect gases strongly impacted by the nanomaterial's surface properties. The process starts when oxygen from the atmosphere is absorbed. Conduction band electrons are drawn to the surface of the TiO_2 NTs grains by the adsorbed oxygen, leaving behind positively charged donor ions. The electrical field becomes stronger when negatively charged oxygen ions like O^- or O^{-2} interact with positively charged donor ions. Therefore, when the amount of oxygen ions on the surface rises, the potential barrier's size also rises, increasing resistance. As a result of interactions with gas molecules in the environment, less O^- or O^{-2} is produced, which lowers resistance [42]. As a result, the TiO_2 NTs gas sensor functions very well at ambient temperature. Since TiO_2 nanotubes are composed of small nanocrystals that have been bonded together to form a 1D tubular structure, this is most likely the case. This suggests that there are a lot of gas chemisorption active sites. TiO_2 nanotubes may also have broad surfaces that can store gas molecules in addition to acting as gas diffusion nanochannels [42].

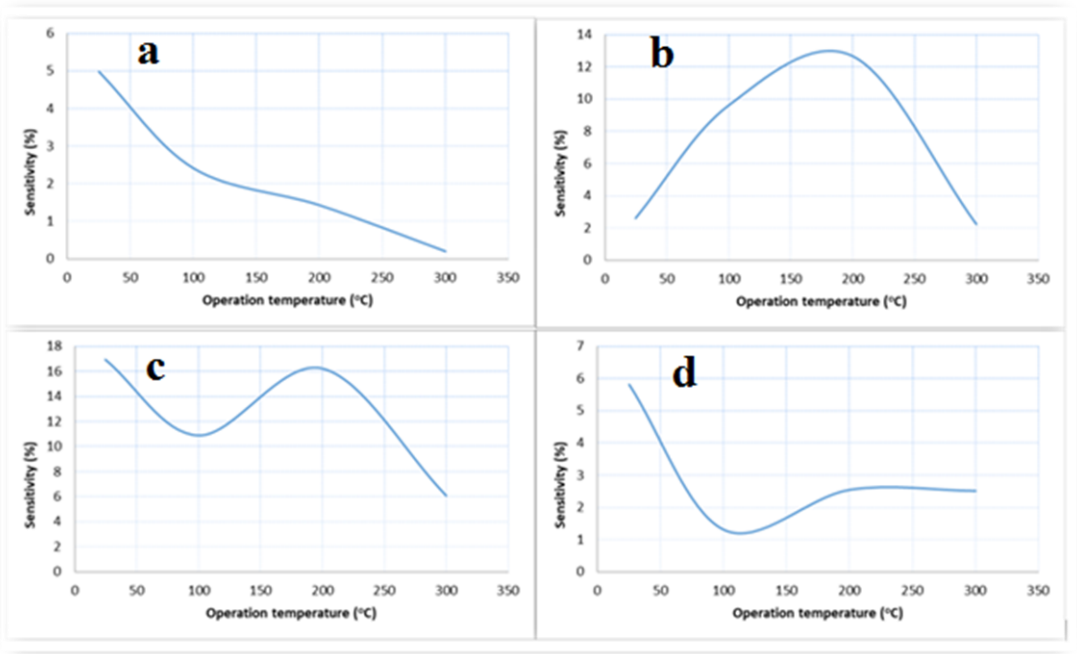

Figure 12: Sensitivity of TiO_2 NTs prepared at: (a) 10 V (b) 20 V, (c) 30 V, and (d) 40 V.

4. Conclusions

In summary, the anodization process was used to produce highly ordered TiO_2 nanotube arrays (TiO_2 NTs). Additionally, this study examined how voltages impacted TiO_2 NTs surface characteristics before having an influence on their capacity to serve as gas sensors. The findings of the gas sensing test showed that TiO_2 NTs at 30 V could detect NO_2 at room temperature with significantly better sensitivity and a quicker response time. The TiO_2 NTs extraordinary efficiency at detecting gases may be primarily attributable to the geometry of their highly ordered nanotubes and the size of their surface area. This study provides the chance to investigate NO_2 sensing by observing the response and recovery durations of NO_2 gas at varied operating temperatures at a constant concentration of 45 ppm. This study shows that the TiO_2 NTs sensor may be improved to detect NO_2 gas with high sensitivity at room temperature.

Acknowledgments

Special thanks are extended to Chemistry Department, College of Science for Women, University of Baghdad, Baghdad, Iraq.

Conflict of Interest

Authors declare that they have no conflict of interest.

References

1. P. Rai, S. Raj, K.-J. Ko, K.-K. Park, and Y.-T. Yu, Sens. Actuat. B: Chem. **178**, 107 (2013).
2. P. Szczepański, R. Kisiel, and R. S. Romaniuk, in Proc. of SPIE, Warsaw University of Technology (Poland) Institute of Microelectronics and Optoelectronics, 2013, p. 890201.
3. D. T. H. To, J. Y. Park, B. Yang, N. V. Myung, and Y.-H. Choa, Sens. Actuat. Rep. **6**, 100166 (2023).
4. K. Nakata and A. Fujishima, J. Photochem. Photobio. C: Photochem. Rev. **13**, 169 (2012).

5. Q. Zhang, E. Uchaker, S. L. Candelaria, and G. Cao, Chem. Soci. Rev. **42**, 3127 (2013).
6. T. J. Awaid, A. K. Ayal, A. M. Farhan, M. S. Sando, and L. Y. Chin, Baghdad Sci. J. **17**, 1183 (2020).
7. H. S. Hreo, A. M. Holi, A. A. Al-Zahrani, A. K. Ayal, and M. Almamari, Bullet. Mat. Sci. **45**, 205 (2022).
8. L. Chin, N. Harun, A. Ayal, Y. Mohd, and L. Pei, Int. J. Eng. Advan. Tech. **9**, 5479 (2019).
9. A. K. Ayal, A. M. Farhan, and Y.-C. Lim, Int. J. Eng. Tech. **7**, 454 (2018).
10. N. A. Samsudin, Z. Zainal, H. N. Lim, Y. Sulaiman, S.-K. Chang, Y.-C. Lim, A. K. Ayal, and W. N. M. Amin, RSC advan. **8**, 23040 (2018).
11. G. Eranna, *Metal Oxide Nanostructures as Gas Sensing Devices*. (Pilani, India, CRC press, 2011).
12. V. Saasa and B. Mwakikunga, Mat. Res. Bull. **164**, 112288 (2023).
13. Q. Fu, K. Lu, N. Li, and Z. Dong, Mat. Res. Bull. **168**, 112457 (2023).
14. O. Sisman, D. Zappa, V.-A. Maraloiu, and E. Comini, Materials **16**, 4802 (2023).
15. A. Kusior, M. Radecka, K. Zakrzewska, A. Reszka, and B. Kowalski, Sens. Actuat. B: Chem. **189**, 251 (2013).
16. Y. Gönüllü, A. A. Haidry, and B. Saruhan, Sens. Actuat. B: Chem. **217**, 78 (2015).
17. Z. Wu, Y. Wang, Q. Wu, X. Cheng, Q. Wang, Y. Yang, B. An, P. Wang, and E. Xie, Appl. Surf. Sci. **614**, 156223 (2023).
18. J. Wu, C. Zhang, Q. Li, L. Wu, D. Jiang, and J. Xia, Sol. Sta. Ionics **292**, 32 (2016).
19. H. Shwetha, S. Sharath, B. Guruprasad, and S. Rudraswamy, Micro Nano Eng. **16**, 100156 (2022).
20. M. D. Fernández-Ramos, L. Capitan-Vallvey, L. Pastrana-Martínez, S. Morales-Torres, and F. Maldonado-Hodar, Sens. Actuat. B: Chem. **368**, 132103 (2022).
21. S. Ma, J. Jia, Y. Tian, L. Cao, S. Shi, X. Li, and X. Wang, Ceram. Int. **42**, 2041 (2016).
22. Y. Gao, D. Kong, J. Han, W. Zhou, Y. Gao, T. Wang, and G. Lu, J. Coll. Inter. Sci. **627**, 332 (2022).
23. X. Wang, S. Li, L. Xie, X. Li, D. Lin, and Z. Zhu, Ceram. Int. **46**, 15858 (2020).
24. S. M. Omran, E. T. Abdullah, and O. A. Al-Zuhairi, Iraqi J. Sci. **63**, 3719 (2022).
25. Y. Shi, X. Li, X. Sun, X. Shao, and H. Wang, J. All. Comp. **963**, 171190 (2023).
26. K. Kim, P. G. Choi, T. Itoh, and Y. Masuda, ACS Appl. Mat. Inter. **12**, 51637 (2020).
27. J.-H. Lee, Sens. Actuat. B: Chem. **140**, 319 (2009).
28. W. A. Al-Taa'y and B. A. Hasan, Iraqi J. Sci. **62**, 4385 (2021).
29. A. K. Ayal, Baghdad Sci. J. **15**, 0057 (2018).
30. A. Kusior, J. Klich-Kafel, A. Trenczek-Zajac, K. Swierczek, M. Radecka, and K. Zakrzewska, J. Eur. Ceram. Soci. **33**, 2285 (2013).
31. R. Dubey, K. V. Krishnamurthy, and S. Singh, Res. Phys. **14**, 102390 (2019).
32. O. Wiranwetchayan, S. Promnopat, T. Thongtem, A. Chaipanich, and S. Thongtem, Mat. Chem. Phys. **240**, 122219 (2020).
33. A. Aboulouard, M. K. Atouailaa, B. Elhadadi, M. Bensemlali, M. Boulghallat, and S. Laasri, Mat. Today: Proce. **66**, 329 (2022).
34. M. Q. Fahem and T. A. Hassan, Iraqi J. Sci. **63**, 4740 (2022).
35. O. V. Otieno, E. Csáki, O. Kéri, L. Simon, I. E. Lukács, K. M. Szécsényi, and I. M. Szilágyi, J. Ther. Anal. Calorim. **139**, 57 (2020).
36. H. Sun, C. Wang, S. Pang, X. Li, Y. Tao, H. Tang, and M. Liu, J. Non-Crys. Sol. **354**, 1440 (2008).

37. M. Gholami, M. Zarei-Jelyani, M. Babaiee, S. Baktashian, and R. Eqra, Ionics **26**, 4391 (2020).
38. A. K. Ayal, A. K. Hashim, A. M. Mohammed, A. M. Farhan, A. M. Holi, and Y.-C. Lim, J. Elect. Mat. **50**, 5161 (2021).
39. M. Radecka, A. Wnuk, A. Trenczek-Zajac, K. Schneider, and K. Zakrzewska, Int. J. Hydro. Ener. **40**, 841 (2015).
40. A. K. Ayal, A. M. Farhan, A. M. Holi, A. A. Al-Zahrani, and Y.-C. Lim, J. Mat. Sci.: Mat. Elect. **34**, 7 (2023).
41. L. Y. Chin, N. Mustaffa, A. K. Ayal, D. Kanakaraju, and L. Y. Pei, J. Chem **23**, 173 (2021).
42. R. Rella, J. Spadavecchia, M. Manera, S. Capone, A. Taurino, M. Martino, A. P. Caricato, and T. Tunno, Sens. Actuat. B: Chem. **127**, 426 (2007).
43. Y. Kwon, H. Kim, S. Lee, I.-J. Chin, T.-Y. Seong, W. I. Lee, and C. Lee, Sens. Actuat. B: Chem. **173**, 441 (2012).
44. H. J. Abdul-Ameer, M. F. Al-Hilli, and F. T. Ibrahim, Iraqi J. Sci. **64**, 630 (2023).
45. S. N. Kareem, M. H. Suhail, and O. G. Abdullah, Tren. Sci. **20**, 5890 (2023).
46. R. M. S. Jarrah, in Journal of Physics: Conference Series, IOP Publishing, 2019, p. 012064.
47. K. Lee, R. Kirchgeorg, and P. Schmuki, J. Phys. Chem. C **118**, 16562 (2014).
48. A. M. Holi, G. Abd Al-Sajad, N. N. Palei, A. A. Al-Zahrani, and A. S. Najm, Nano Biomedic. Eng. **14**, 7 (2022).
49. P. Bindra, S. Gangopadhyay, and A. Hazra, IEEE Sens. J. **20**, 664 (2019).
50. G. Yang, M. Zhang, D. Dong, X. Pan, Y. Zhou, S.-T. Han, Z. Xu, W. Wang, and Y. Yan, J. Mat. Chem. C **7**, 11118 (2019).

توليف الأنابيب النانوية TiO_2 كمستشعر لغاز ثنائي اوكسيد النتروجين الخطر بطريقة كهروكيميائية

مينا محمد فارس[1] و اسماء كاظم عيال[2]
[1]قسم الكيمياء، كلية العلوم، جامعة بغداد، بغداد، العراق
[2]قسم الكيمياء، كلية العلوم للبنات، جامعة بغداد، بغداد، العراق

الخلاصة

بسبب النمو السريع للاجهزة الكهربائية المستخدمة في الكشف عن الغازات الضارة، زادت أهمية أجهزة استشعار الغاز. يمكن استخدام انحراف الأشعة السينية لفحص بنية الطور البلوري لمواد االمستشعر التي تؤثر على خصائص تحسس الغاز. حيث يساهم هذا في دراسة تأثير التوليف الكهروكيميائي لمواد ثاني أكسيد التيتانيوم (TiO_2) مع اطوار بلورية مختلفة، مثل (rutile TiO_2 (R- TiO_2NTs و anatase TiO_2 (A- TiO_2NTs). في هذا العمل، درسنا تأثير الجهد لتحضير الأنابيب النانوية TiO_2عبر تقنية الأنودة لتطبيقات مستشعرات الغاز. توضح النتائج التي تم الحصول عليها من تحليل انحراف الأشعة السينية (XRD) والتحليل الطيفي لتشتت الطاقة (EDX) والفحص المجهر الإلكتروني الماسح (FE-SEM) أنه تم تكوين TiO_2. بالإضافة إلى ذلك، تم إجراء فحص منهجي لخصائص الكشف عن الغاز. حيث تم إنتاج مستشعر الغاز من أنبوب TiO_2النانوي، وتم توجيه ميزات الكشف عن الغاز إلى ثاني أكسيد النيتروجين (NO_2)، وهو غاز خطير. يتحسس المستشعر الذي يتكون من الأنابيب النانوية TiO_2غاز ثاني أوكسيد النيتروجين جيدًا عند درجات حرارة مختلفة من درجة حرارة الغرفة إلى 300 درجة مئوية بالإضافة إلى أنه يتمتع بحساسية جيدة لهذا الغاز. تظهر النتائج أن مستشعر الغاز الذي تم تصنيعه عند 30 فولت لديه حساسية جيدة ووقت استجابة قصير في درجة حرارة الغرفة لاستشعار غاز ثاني أوكسيد النيتروجين.

الكلمات المفتاحيه: أنابيب TiO_2 النانوية، الطريقة الكهروكيميائية، غاز ثاني أكسيد النيتروجين (NO_2)، استشعار الغاز، الحساسية.